PERGAMON

Chemical Engineering Science 54 (1999) 5809–5821

Chemical Engineering Science

DEM simulation of fluidized beds for gas-phase olefin polymerization

Yasunobu Kaneko[a,*], Takeo Shiojima[a], Masayuki Horio[b]

[a]*Production Technology Center, Idemitsu Petrochemical Co., Ltd., Ichihara, Chiba 299-0193, Japan*
[b]*Department of Chemical Engineering, Tokyo University of Agriculture and Technology, Koganei, Tokyo 184-8588, Japan*

Received 6 August 1998; received in revised form 22 January 1999; accepted 9 March 1999

Abstract

The temperature behavior of particles and gas in a fluidized bed reactor for polyolefin (PO, i.e., polyethylene (PE) and polypropylene (PP)) production was numerically analyzed based on the Discrete Element Method (DEM). Simulation was performed using a numerical code (modified SAFIRE code) by modifying SAFIRE ver.1 of Mikami, Kamiya and Horio (1998, *Chemical Engineering Science, 53*, 1927–1940) by incorporating the energy balance and the reaction rate. Heat transfer from a particle to gas was estimated using the Ranz–Marshall equation. The reaction rates were calculated by Arrenius type zero-th order kinetic expressions including the effect of catalyst weight. Hot spot formation at the bottom corner immediately above the perforated plate distributor was observed even when an equal amount of monomer gas was fed to all orifices. When the gas was not uniformly supplied, rather stable particle swirls formed in the bed creating a hot spot at the core of each swirl. The degree of mixing was found an effective parameter to predict the hot spot formation.

Keywords: Polyolefin; Discrete element method; Polymerization; Fluidization; Gas phase; Numerical simulation

1. Introduction

Polyolefins (POs), especially polypropylene (PP) and polyethylene (PE), have been the most popular resins due to their advantages including low price, flexibility of molding and ease of disposal or recycling. The annual production of PP is more than 20 million tons/year throughout the world, and more than 2.5 millions ton/year of PP and more than 3.0 millions ton/year for PE in Japan including low density polyethylene (LDPE), linear low density polyethylene (LLDPE), ethylene vinyl acetate copolymer (EVA) and high density polyethylene (HDPE). It is expected that the demand for PP and PE is likely to increase further in the future. Because there is no need for drying and separation of atactic polypropylene from solvents, a gas-phase PO polymerization process is more advantageous than conventional liquid slurry processes. Therefore, a large proportion of PO has recently been manufactured in gas-phase reactors that commonly employ Ziegler–Natta catalysts of high activity and selectivity. Three reactor types commercialized so far are the fluidized bed type, e.g., the UNIPOL process (USA), the vertical type with a helical ribbon agitator, e.g., the NOVOLEN process (Germany), and the horizontal vessel type with a multi-paddle agitator, e.g., the AMOCO process (USA). Every reactor type has both advantages and disadvantages, but fluidized-bed reactors with no agitators have been more widely accepted worldwide for PO production. This is because agitators and the mechanical seals of their drive shafts tend to limit the reactor scale.

In gas-phase polymerization, each polymer particle grows up around a catalyst particle. Monomers penetrate into the polymer layer to the active sites on the catalyst and react with the polymer centering around the sites. Because polymerization is exothermic in nature, the temperature of the polymer particles tends to rise and sometimes to exceed the melting point of the polymer (roughly 430 K for PP homopolymer and 400 K for high-density PE), unless the particles are not sufficiently cooled. Under poor cooling conditions, polymer particles melt and form lumps which may then cause defluidization. Polymer particles may also burst because of the evaporation of dissolved monomer and produce unwanted small disintegrated particles. Remarkable progress has been made recently in catalyst activity and product grades. The increasing catalyst activity and the

* Corresponding author.
E-mail address: 25007828@ipc.idemitsu.co.jp (Y. Kaneko)

0009-2509/99/$ - see front matter
PII: S0009-2509(99)00153-0

increasing ethylene content of the random copolymer enhance the reaction rate; therefore, the control of PO reactors is becoming even more important.

The importance of heat removal from a PO reactor has been recognized from an industrial viewpoint. Heat transfer around a polymer particle was investigated by Floyd, Choi, Taylor and Ray (1986a, b), Floyd, Heiskanen, Tomi, Taylor, Mann and Ray (1987), Hutchinson and Ray (1990, 1991), Hutchinson, Chen and Ray (1992), McKenna, Dupuy and Spitz (1995, 1997) and McKenna, Barbotin and Spitz (1996) using multigrain models. However, these studies were on kinetic aspects, and the behavior of polymerization reactors must be studied in consideration of particle and fluid dynamics in the reactor. Because of the difficulties in both experiments and mathematical analysis, there has been little published information available on this key issue.

However, the potential application of the numerical tools that have become available recently in the particle technology field would provide valuable information concerning the dynamic phenomena taking place in fluidized bed reactors. The discrete element method (DEM) with the soft sphere assumption, particularly, the Mikami et al. (1998) SAFIRE code (Simulation of Agglomerating Fluidization in Industrial Reactor Engineering) has been proven quite powerful for realistic simulation of fluidized beds. In the DEM simulation one can avoid using a particle stress tensor which is almost impossible to determine for powders in industrial fluidized beds. Accordingly, in the present paper an attempt is made to apply the DEM to PO reactors taking into account the polymerization reaction kinetics, temperatures of individual particles and gas–solid heat exchange to provide numerical information particularly on the mechanism of hot spot formation in the fluidized bed.

2. Theoretical

2.1. Assumptions

A mathematical model was developed based on the following assumptions for simplification:
Assumptions same as SAFIRE ver.1:

1. Gas is inviscid except for gas–particle vicinity.
2. Particles are assumed to be spheres of equal size.
3. The bed is two dimensional with thickness equivalent to one particle diameter. The front and back walls were assumed to be frictionless.
4. Particles have a soft sphere interaction with a Hookian linear spring and a dash pot allowing multiple particle contacts under a Coulomb type friction condition.
5. Viscous damping effect is only indirectly included by taking into account inelastic collisions.

Additional assumptions for the present work:

6. Particle-to-particle adhesion force is negligible.
   This assumption is just for simplification to focus our attention on the thermal aspects.
7. Physical properties such as heat capacity, thermal conductivity, density and viscosity of the gas and the particles are assumed to be constant. Values are calculated for the initial temperature, i.e., 343 K for PP and 363 K for PE.
8. Gas volume change due to reaction is neglected because it should be small compared with the total fluidizing gas flow rate.
9. Heat loss through the reactor wall is neglected.
10. Heat conduction in the gas phase is neglected except in the particle vicinity.
11. Temperature is uniform in each particle.
    This is also for simplification, but in the present cases, the Bio number ($Bi \equiv \lambda_p/(h_p \cdot d_p)$) is well below unity. For instance, for a PP particle $\lambda_p = 0.11\ \mathrm{Jm^{-1}\ s^{-1}\ K^{-1}}$, $d_p = 1 \times 10^{-3}$ m, $h_p \approx 0.42 \times 10^3\ \mathrm{Jm^{-2}\ s^{-1}\ K^{-1}}$ and $Bi = 0.26$.
12. For the particle-to-gas heat transfer coefficient, the Ranz–Marshall correlation (1952) is applied for the local condition of each particle.
    This assumption is only for simplification because such a semi-classical approach would not be adopted in a future simulation where the microscopic picture of the boundary layer around each particle is taken into consideration.
13. Direct particle-to-particle heat transfer is neglected.
    This assumption is consistent with Assumptions 1, 5 and 12. To take into account the particle-to-particle heat transfer, we have to pay more careful attention to particle–particle collision with a focus on viscous damping by the thin fluid film between colliding particles, probably by direct Navier–Stokes simulation. However, the main objective of the present study is to investigate the major issue of commercial operation, the mechanism of hot spot and lump formation, and to evaluate the maximum possible temperature rise based on the available DEM technique. Although the temperature rise in the particle phase predicted by a model using Assumption 13 should be a little larger than that in reality, it could provide us with mechanistic information on hot spot formation.
14. Spring constant is adjusted only from the viewpoint of numerical economy.

According to Tsuji, Kawaguchi and Tanaka (1993), the spring constant is a flexible parameter in the simulation of macroscopic hydrodynamics of fluidized beds. However, because the physical

properties they assumed for the bed material were quite different from those of the material in the present study, it may be worth examining the influence of the spring constant on fluidization behavior concerning a polymerization condition. In Fig. 1(a)–(c) snapshots of the fluidization behavior are shown for the cases of spring constants of 8, 800 and 80 000 N/m, respectively. The remaining conditions are the same as those of Fig. 5(a) in a later section. Because the spring constant did not affect the macroscopic bed behavior even under polymerization conditions and because we are avoiding the inclusion of the particle-to-particle heat transfer as well as the macroscopic collision characteristics, $k = 800$ N/m is adopted in the following calculation.

2.2. Governing equations

The governing equations for gas phase and particle motion are almost the same as those given by Mikami et al. (1998) as summarized in Appendix A except for the gravity term in the gas momentum equation and the buoyancy force in the particle momentum equation.

For energy balance, the following equation is derived:

$$\frac{\partial(\varepsilon T_g)}{\partial t} + \frac{\partial(\varepsilon u_i T_g)}{\partial x_i} = \frac{Q_g}{\rho_g c_{p,g}}, \tag{1}$$

where $c_{p,g}$ is the heat capacity of the gas and T_g is the gas temperature. Q_g is the heat transfer rate between a particle and the gas in a unit volume and is expressed by the

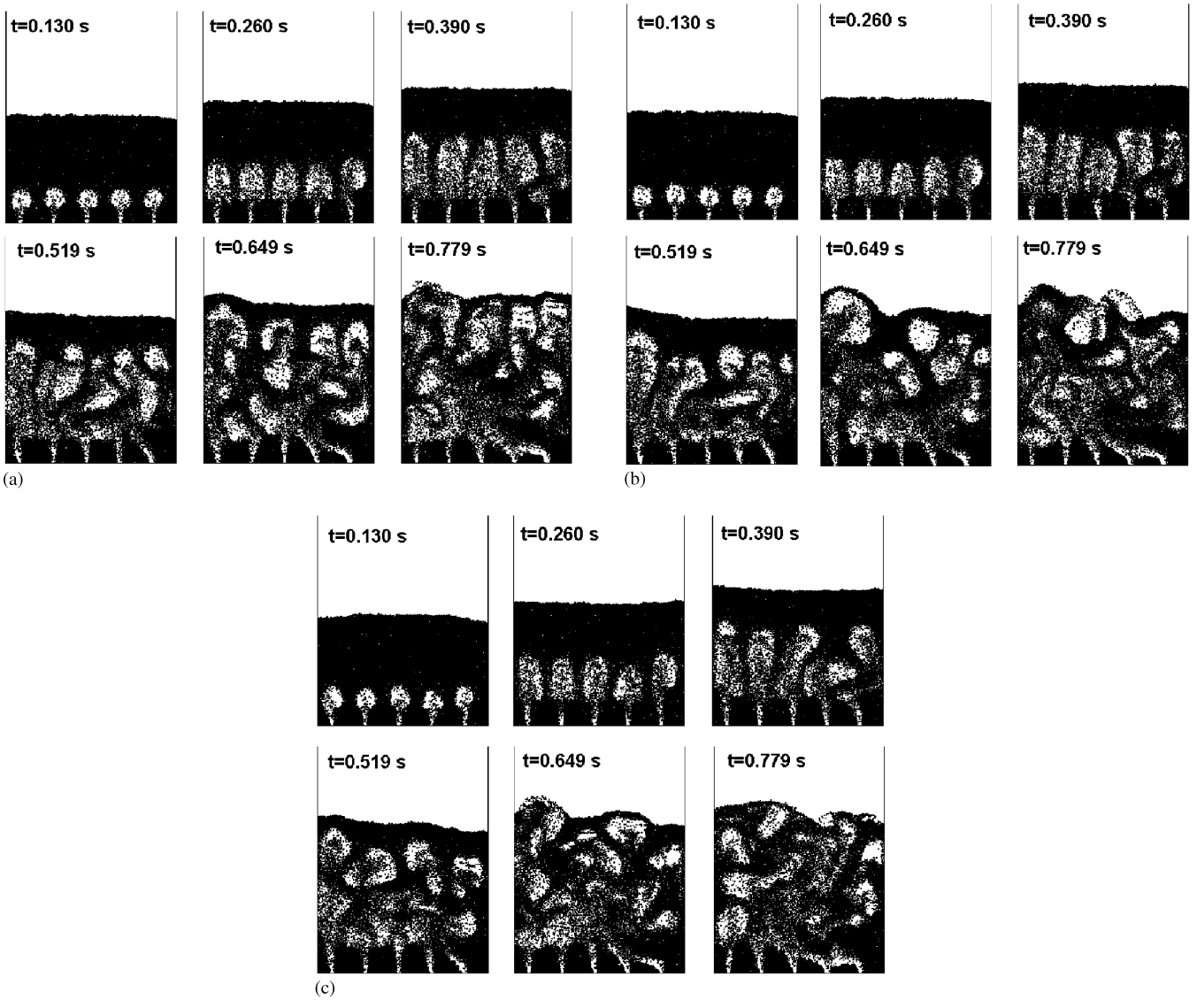

Fig. 1. Snap shots of fluidization behavior (Propylene polymerization, Number of particles = 14,000, $u = 3u_{mf}$). (a) $k = 8$ N/m. (b) $k = 800$ N/m. (c) $k = 80{,}000$ N/m.

following equation according to assumptions 2, 9, 11 and 13:

$$Q_g = \frac{6\cdot(1-\varepsilon)}{d_p}\langle h_p(T_p - T_g)\rangle \tag{2}$$

where h_p is the heat transfer coefficient between a particle and the gas, d_p is the particle diameter and T_p is the temperature of a particle in the fluid cell. The notation $\langle\ \rangle$ implies the local ensemble averaging. Heat transfer coefficient h_p is estimated by the following Ranz–Marshall correlation (Ranz, 1952):

$$Nu = 2.0 + 0.6\,Pr^{1/3}Re_p^{1/2} \tag{3}$$

where

$$\begin{aligned} Nu &= h_p d_p/\lambda_g \\ Pr &= c_{p,g}\mu_g/\lambda_g \\ Re_p &= \rho_g d_p|u - v_l|/\mu_g \end{aligned} \tag{4}$$

λ_g is the thermal conductivity of the gas, $c_{p,g}$ is the heat capacity of the gas, μ_g is the gas viscosity and $|u - v_l|$ is the gas-to-particle relative velocity.

The reaction rate expression of Floyd et al. (1986b) for a typical $TiCl_3$ type which was defined per catalyst volume is converted to the following expression for one polymer particle:

$$R_p = k_{p0}\exp\left(-\frac{E}{RT_p}\right)w_c p_r \tag{5}$$

where k_{p0} is the preexponential factor of the polymerization rate coefficient, E is the activation energy for polymerization, w_c is the weight of catalyst in a particle and p_r is the monomer gas pressure. The parameters k_{p0} and E were determined from the experimental data separately obtained using a batch autoclave reactor.

In the present calculation, the particle size change is negligible because the simulation is done only for a short period. Accordingly, the temperature change dominates the change in the reaction rate. In the future simulation for cases with a wide size distribution of polymer particles, a kinetic expression including monomer diffusion resistance may have to be applied.

In order to adjust the reaction temperature, catalyst weight w_c is determined by the following energy balance:

$$w_c = \frac{1}{n_t}\frac{V_g\rho_g c_{p,g}(T_{g,o} - T_{g,i})}{k_{p0}\exp\left(-\frac{E}{RT_{p,0}}\right)p_r(-\Delta H_r)} \tag{6}$$

where n_t is the number of particles in a bed, V_g is the volumetric gas flow rate, $T_{p,0}$ is the initial particle temperature and $T_{g,i}$ and $T_{g,o}$ are the inlet and outlet gas temperatures, respectively. To determine the value of w_c, a set of ordinary values of $T_{p,0}$, $T_{g,i}$ and $T_{g,o}$ was chosen.

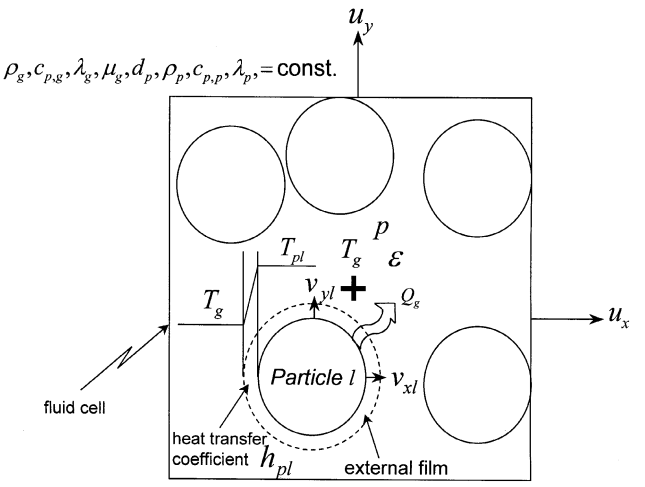

Fig. 2. Variables defined in a cell for the energy balance.

The energy balance for a particle is given by the following equation:

$$V_p c_{p,p}\rho_p\frac{dT_p}{dt} = R_p(-\Delta H_r) - \{h_p(T_p - T_g)S_p\}, \tag{7}$$

where V_p is the volume of a particle, $c_{p,p}$ is the specific heat of the solid, $(-\Delta H_r)$ is the heat of polymerization and S_p is the external surface area of a particle.

2.3. Numerical algorithm

Fig. 2 illustrates the fluid cell employed for numerical computation and the variables defined for energy balance in the gas phase. Gas velocity is defined at the center of each cell-to-cell boundary plane to eliminate numerical instability. Voidage, gas pressure and gas temperature are defined at the center of the cell. To solve the equations of fluid motion Eqs. (A.1), (A.2) and (1), the SIMPLE (Semi-Implicit Method for Pressure-Linked Equations) algorithm and the explicit method with the upwind scheme were adopted. The computation scheme for calculating voidage ε in each fluid cell in the present simulation code is depicted in Appendix B.

The time step for stable calculation is determined by the following equation of Tsuji et al. (1993):

$$\Delta t = \frac{1}{5}2\pi\sqrt{\frac{m}{k}} \tag{8}$$

where Δt is the time step, m is the mass of a particle and k is the spring constant.

3. Computation conditions

Computation conditions and physical and additional parameters used are shown in Tables 1 and 2, respectively.

The reactor width (x-direction) was divided into 41 cells. A personal computer (Fujitsu Ltd., FMV-6266T6) was used for calculation. The physical properties in Table 2 are those taken at 343 K and 3.1 MPa for PP and 363 K and 2.1 MPa for PE. To examine the pressure effect on the bubbling behavior, calculations were done also for the ambient condition.

For a PP reactor, the gas inlet temperature $T_{g,i}$ as well as the initial particle temperature $T_{p,0}$ were assumed to be 343 K. To determine the catalyst weight in each particle $T_{g,o} = 345$ K was substituted into Eq. (6). In accordance with this, the average temperatures of the particles and the outlet gas became roughly 3 K higher than the inlet gas temperature after several seconds.

For the case of PE reaction, the inlet gas temperature is generally much lower than that of PP reaction because the boiling point of ethylene is much lower than that of propylene. A typical inlet gas temperature is 293–303 K in commercial scale polyethylene production plants. Hence the inlet gas temperature for calculation in the case of polyethylene was set at 293 K. $T_{g,o}$ and the initial particle temperature $T_{p,0}$ were set at 363 K, which was the typical ethylene polymerization temperature.

Table 1
Computation conditions

Particles	
Number of particles, n_t	14,000, 28,000
Particle diameter, d_p	1.0×10^{-3} m
Restitution coefficient, e	0.9
Friction coefficient, μ	0.3
Spring constant, k	800 N/m
Bed	
Bed size	0.154×0.3825 m (for $n_t = 14{,}000$) 0.154×0.765 m (for $n_t = 28{,}000$)
Types of distributor	porous plate, perforated plate
Number of fluid cells	41×105 (for $n_t = 14{,}000$) 41×210 (for $n_t = 28{,}000$)
Time step	Polypropylene 1.298×10^{-5} s Polyethylene 1.346×10^{-5} s

4. Results and discussion

4.1. Effect of pressure on fluidization behavior

Fig. 3 shows the snapshots of the bubbling behavior for the PP particles under both ambient and high pressure conditions. It is seen from the snapshots that the bubble diameter decreases at elevated pressure. This result shows that bubbles do not grow much while rising in the bed at elevated pressure. The CPU time required for computation of the corresponding real time is shown in Table 3. The computation time in the case of PP or PE reaction is shorter than that of PP under ambient condition with no reaction. Because the computation loop to judge if a particle is contacting a neighboring particle is included in the SAFIRE code to reduce the computation time, the computation time decreases with decreasing total number of particle–particle contact points. Accordingly, the shorter computation time for the elevated

Table 2
Parameters for computation

			Propylene reaction		Ethylene reaction
Particles	density, ρ_p	kg/m^3	667		717
	specific heat, $c_{p,p}$	J/kg/K	1.67×10^3		2.30×10^3
	initial temperature, $T_{p,0}$	K	343		363
Gas	density, ρ_g	kg/m^3	74.84		20.44
	viscosity, μ_g	Pa s	1.0×10^{-5}		1.0×10^{-5}
	thermal conductivity, λ_g	J/m/s/K	2.09×10^{-2}		2.91×10^{-2}
	specific heat, $c_{p,g}$	J/kg/K	1.67×10^3		1.80×10^3
	inlet gas temperature, $T_{g,i}$	K	343		293
	pressure, p	MPa	3.1		2.1
Reaction	rate constant, $k_p o$	kg-PP/s/Pa/kg-cat		8.948×10^{-6}	
	activation energy, E	J/mol		10585	
	catalyst weight, w_c	kg/m^3	7.0×10^{-10}		4.2×10^{-9}
	heat of polymerization, $(-\Delta H_r)$	J/kg	2.51×10^3		3.77×10^3
u_{mf}	predicted (Wen–Yu)	m/s	0.052		0.101
	estimated by simulation	m/s	0.066 (at ambient condition: 0.29 m/s)		0.112

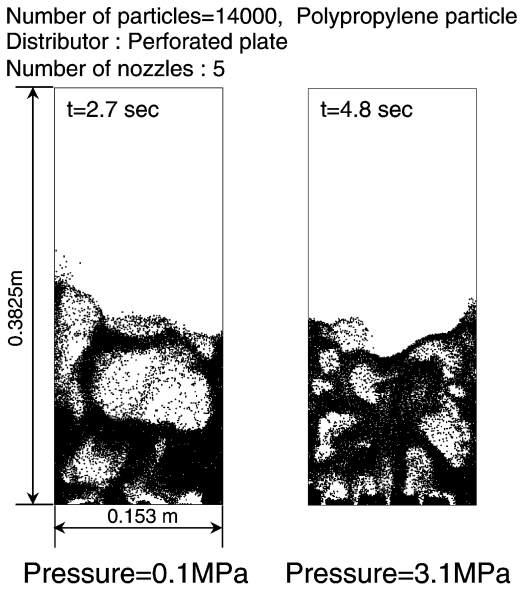

Fig. 3. Fluidization behavior at elevated pressure ($u = 3u_{mf}$) (time t shown is after the initiation of fluidization).

Table 3
CPU time for computation

	CPU time	Real time
PP, PE reaction	About 12 h	1 s
PP ambient condition (without reaction)	About 20 h	1 s

(Computer used: FMV-6266T6)

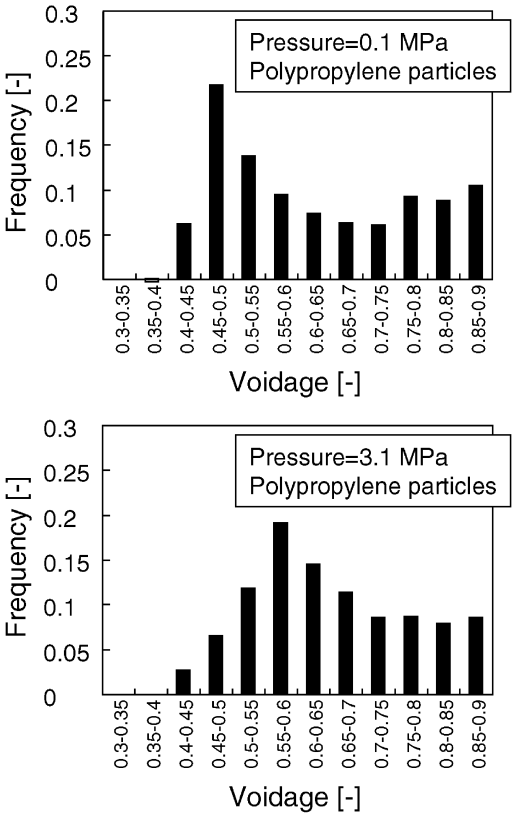

Fig. 4. Frequency distribution of voidage.

pressure conditions suggests that the voidage in the emulsion phase in the bed at an elevated pressure is larger than that under ambient condition. To clarify this point, the frequency distributions of bed voidage were obtained by dividing the voidage of each fluid cell by the total number of fluid cells excluding the fluid cell having $\varepsilon > 0.9$. The results are shown in Fig. 4. The peak voidage in the frequency distribution corresponds to the most frequent voidage in the dense phase. The peak voidage ($\varepsilon_{peak} = 0.55$–$0.6$) of the dense phase under elevated pressure condition is higher than that ($\varepsilon_{peak} = 0.45$–$0.5$) under ambient condition.

4.2. Simulation results on temperature dependent behavior

Typical results for particle and gas temperatures obtained for PP reaction conditions are shown in Fig. 5 for two different bed heights, where particles and fluid cells are colored according to their temperatures. From this figure, it can be seen that the gas temperature in the bubble phase was 2–3 K less than that in the emulsion phase. In the emulsion phase, both the temperatures of the particles and the gas were almost the same, indicating quick heat exchange between gas and particles. Fig. 6 shows similar results for a PE condition. The temperature of the particles located at the position of relatively low gas temperature is also lower than that in other areas.

Fig. 7(a) and (b) show longitudinal temperature profiles of the particles and gas for PP and PE, respectively, for the case of a porous plate distributor. A steep gradient of bed temperature was found near the bed bottom. Above this area, the bed temperature was almost constant. Due to the difference in the heat of reaction, the temperature gradient was steeper in the PE reactor than in the PP reactor.

4.3. Influence of distributor design on hot spot formation

Fig. 8 shows snapshots of particle and gas temperatures for both porous plate and perforated plate distributors to examine the influence of the distributor types. For the case of the perforated distributor, a dead zone of particles appeared at the corner of the distributor where particle and gas temperatures continuously increased during calculation. In the case of the porous plate distributor, there was no high temperature zone in the

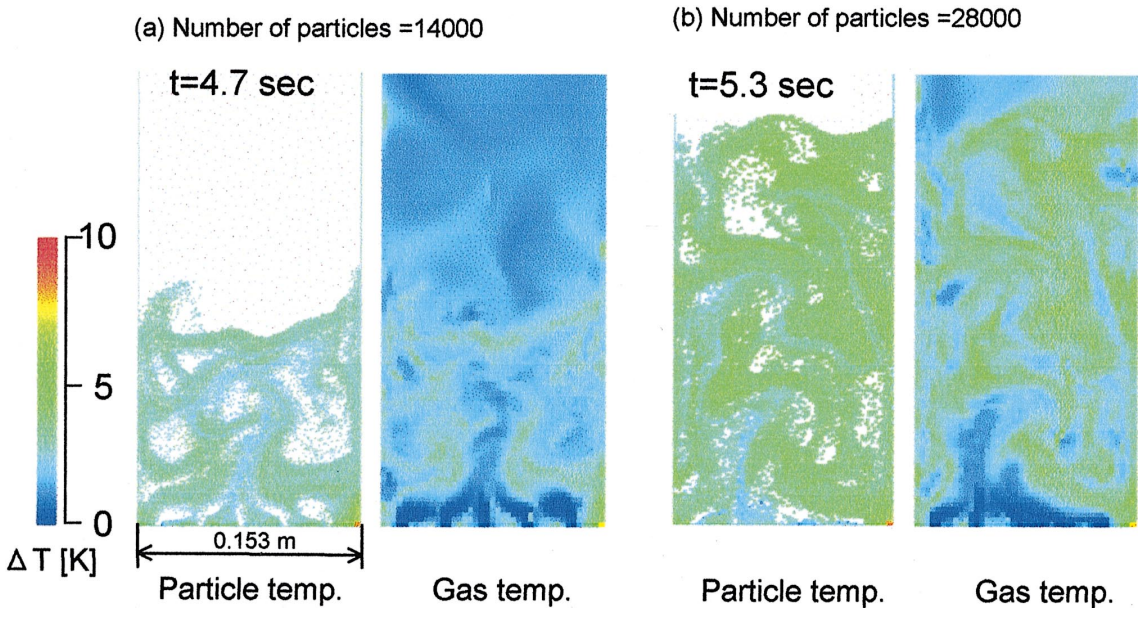

Fig. 5. Typical snapshots of temperature distributions of particle and gas ($u = 0.156$ m/s) (reaction: Propylene polymerization, gas inlet temp. = 343 K, Perforated plate distributor: 5 holes).

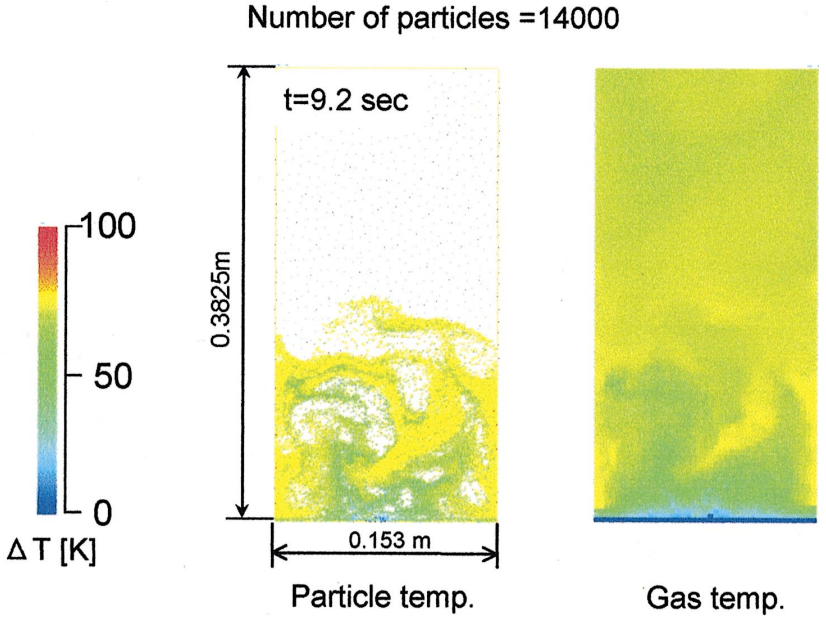

Fig. 6. Typical snapshots of temperature distributions of particle and gas ($u = 0.303$ m/s) (reaction: Ethylene polymerization, gas inlet temp. = 293 K, Porous plate distributor).

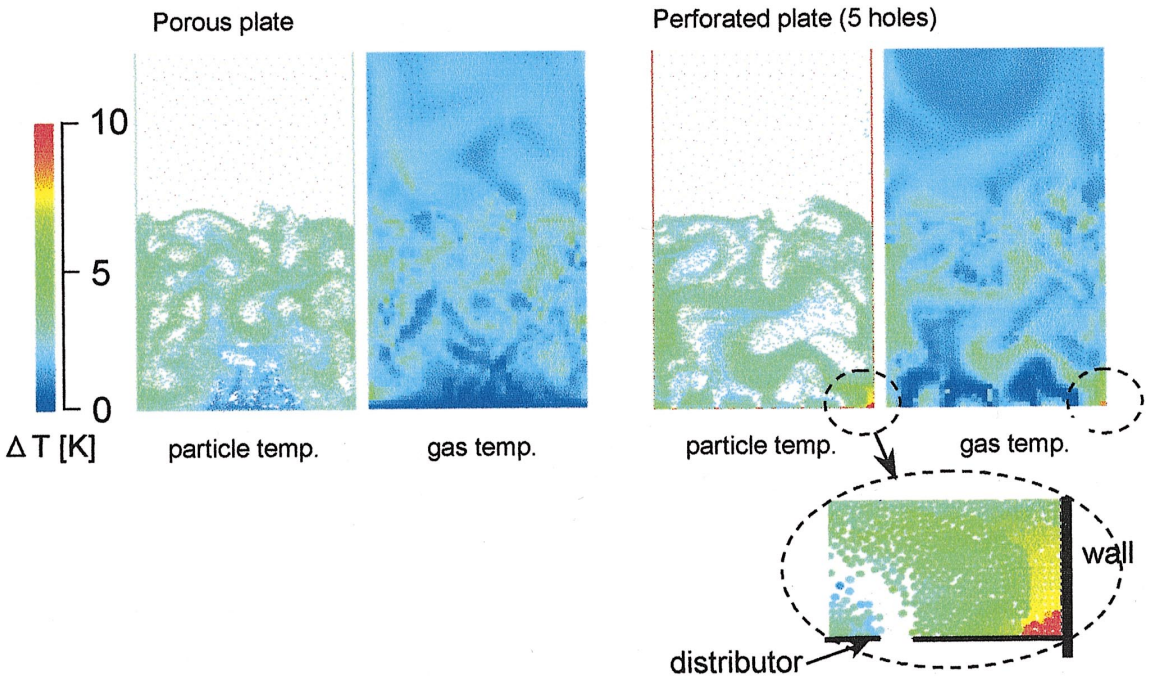

Fig. 8. Influence of distributor on particle and gas temperatures (Number of particles = 14000, PP reaction, $u = 3u_{mf}$, $t = 6.2$ s).

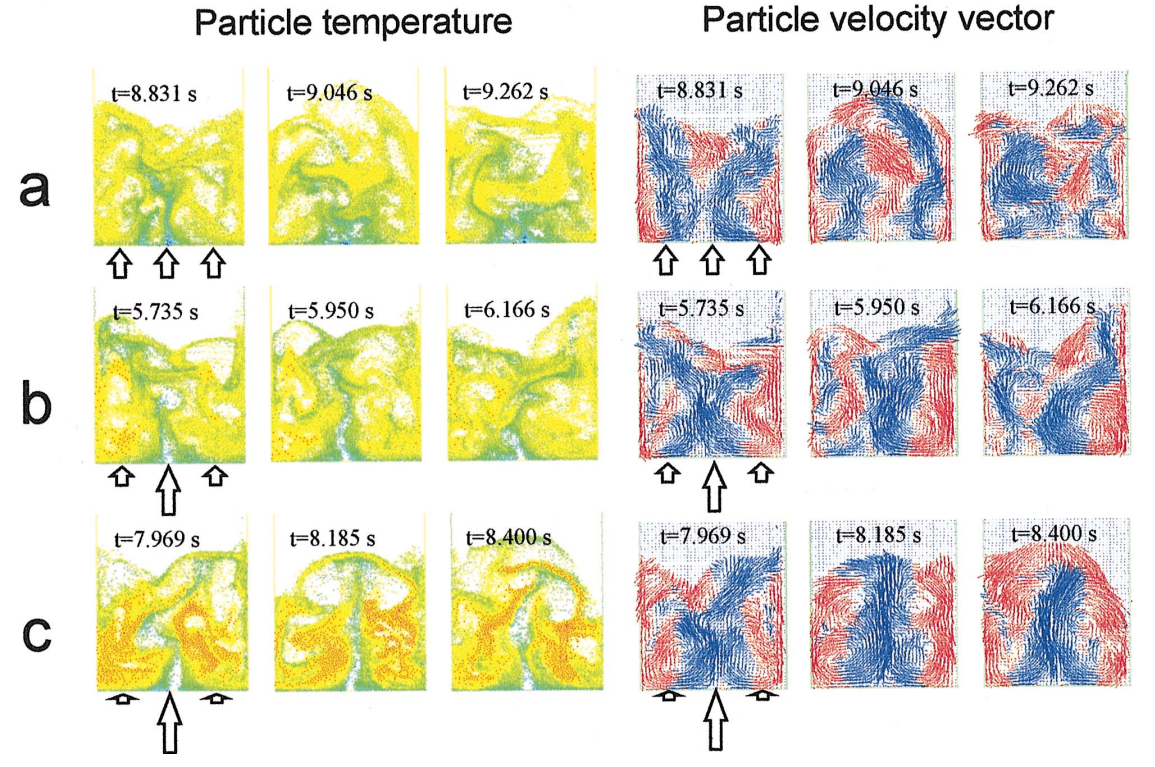

Fig. 9. Effect of non-uniform gas supply on particle temperature distribution (Number of particles = 14000, Ethylene polymerization, $u = 3u_{mf}$).

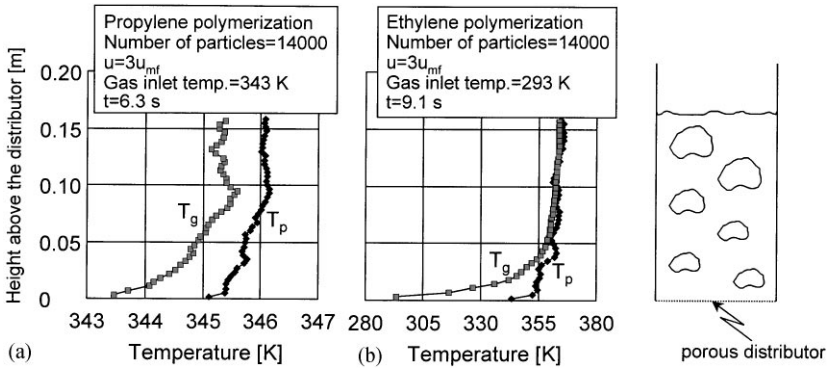

Fig. 7. Vertical profiles of particle and gas temperatures for the case of porous plate distributor.

fluidized bed. This is in good agreement with the previous observations in many patents (Showadenko, 1991; Sumitomo Chemical, 1997; Montedison, 1985) where the importance of distributor design in preventing the dead zone formation has been stressed.

4.4. Influence of particle behavior on hot spot formation

Hot spot formation is not always limited to that in the dead zone on the distributor. In a large commercial scale reactor, it is reported that the bed particle circulation induced by bubble motion often causes hot spot formation in the center of particle revolution (Raufast, 1984). In order to examine whether DEM simulation can reproduce such an observation, particle circulation was artificially generated by feeding gas nonuniformly from the nozzles. Fig. 9 shows temperature and solid velocity distributions for three different cases of gas distribution for the same average fluidizing gas velocity. The particle velocity vector is shown by blue and red lines representing the upward and downward flow directions, respectively. In the case of Fig. 9a, the superficial gas velocity u_y was three times as large as u_{mf} for all bottom cells, i.e., uniform gas feeding. In the case of Fig. 9b, u_y was set at $9.33u_{mf}$ for the three center cells and for the other 38 side cells at $2.5u_{mf}$. In the case of Fig. 9c, u_y was set at $15.67u_{mf}$ for the three center cells and for the other 38 side cells at $2.0u_{mf}$.

As can be clearly seen in Fig. 9a–c, the more the gas injection was localized, the higher became the hot spot temperature. This temperature nonuniformity seems to be related to the randomness of particle mixing. In Fig. 9a, the particle eddy center moved around in the bed due to the random bubble motion. However, in Fig. 9b and c, particularly in c, it can be seen that rather stable particle circulation eddies were induced by the non-uniform gas injection. In the region of lower particle velocity, particle temperature is much higher than that in the other remaining regions and it is even above the softening temperature of PE. This result indicates that the random mixing of particles is important for the temperature nonuniformity and for smooth and safe operation of polyolefin synthesis reactors, especially when the heat of reaction is high.

To clarify the above point further, the degree of mixing M (Satoh, Deguchi, Komura & Miyanami, 1985; Muguruma, Tanaka, Kawatake & Tsuji, 1996), defined by the following equation, was calculated to evaluate the influence of the intensity of particle mixing on particle temperature:

$$M = \frac{\sigma}{\sigma_0}, \tag{9}$$

$$\sigma = \sqrt{\frac{1}{N-1}\sum_{i=1}^{N}(C_i(t) - \bar{C})^2}, \tag{10}$$

$$\sigma_0 = \sqrt{\bar{C}(1-\bar{C})}, \tag{11}$$

where σ is the standard deviation at $t = t$, σ_0 is the standard deviation before mixing, N is the number of measuring cells, $C_i(t)$ is the concentration of tracer particles in the measuring cell i at $t = t$ and $\bar{C}$ is the concentration of tracer particles in the bed. The standard deviation of tracer particle concentration for a perfect mixing condition is expressed as:

$$\sigma_r = \sqrt{\frac{\bar{C}(1-\bar{C})}{\bar{n}}} \tag{12}$$

where $\bar{n}$ is the average number of particles contained in a sampling cell. A sampling cell is defined by dividing the fluidized column into 20×52 parts so that its volume is almost equivalent to four fluid cells. It should be noted here that if there is no particle in a sampling cell, $C_i(t)$ is not available and that if there are only a few particles in a sampling cell, the error in the standard deviation value is large. Accordingly, the sampling cells in which more than ten particles are contained were chosen to determine the degree of mixing. To eliminate the influence of initial conditions, M was calculated at $t = 6.0$ s after the average particle temperature became nearly stable. Particles located below 0.03642 m, i.e., 10 fluid cells from

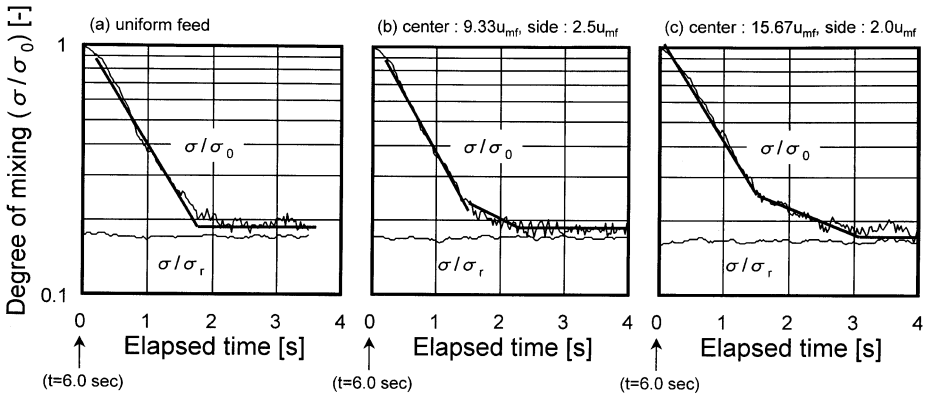

Fig. 10. Mixing curves.

the bed bottom, were defined as tracer particles. Accordingly, the values of $\bar{C}$ were about 0.5 in all three cases.

Fig. 10 shows the change in $\sigma/\sigma_0(=M)$ and σ/σ_r (degree of mixing for perfect mixing) for the three cases mentioned above. The initial steep decrease in σ/σ_0 indicates the effect of convective mixing by bubble motion. Its inclination indicates the mixing rate constant. The rate constant decreased, although only slightly, with the increasing nonuniformity of gas injection. However, in Fig. 10c, there is a slow mixing period between 1.5 and 2.5 s indicating the diffusive or share mixing of particles. All σ/σ_0 curves finally reached the equilibrium σ/σ_r line. Obviously, the strong stable particle revolution in nonuniform gas feeding is the major cause of the slower mixing and larger temperature nonuniformity. Accordingly, the degree of mixing is recommended for prediction of hot spot formation.

5. Conclusions

A DEM simulation code incorporated with the reaction and energy balances was developed based on the soft sphere interaction at particle collision for a fluidized-bed olefin polymerization reactor. The results are fairly realistic concerning particle and gas temperature behavior and also the bubbling behavior in a gas fluidized bed at elevated pressure.

Hot spot formation was observed on the distributor near the wall of the fluidizing column. When a large stable particle revolution flow is formed in the bed, a hot spot was found to form quickly. It was also found that the degree of mixing can be used as an effective index to identify and prevent hot spot formation.

Notation

Bi	bio number, dimensionless
$\bar{C}$	concentration of tracer particles in the bed, dimensionless
$C_i(t)$	concentration of particle in sampling cell i, dimensionless
$c_{p,g}$	gas heat capacity, J/kg/K
$c_{p,p}$	specific heat of solid, J/kg/K
C'_D	modified drag coefficient, dimensionless
d_p	particle diameter, m
e	restitution coefficient, dimensionless
E	activation energy for polymerization, J/mol
f_i	gas-particle interaction force acting on a fluid cell, N
F_n	normal soft sphere interaction force at contact, N
F_{pi}	particle-gas interaction force, N
F_t	tangential soft sphere interaction force at contact, N
g	gravity acceleration, m/s^2
h_p	heat transfer coefficient between the particle and its external gas, J/K/m^2/s
$(-\Delta H_r)$	heat of polymerization, J/kg-PP
I	moment of inertia, kg m^2
k	spring constant, N/m
k_{p0}	preexponential factor of the polymerization rate coefficient, kg-PP/s/Pa/kg-cat
l	particle number, dimensionless
m	mass of particle, kg
M	degree of mixing, dimensionless
n	number density of particle, m^{-3}
$\bar{n}$	average number of particles in a sampling cell, dimensionless
n_t	number of particles in a bed, dimensionless
N	number of sampling cells, dimensionless
Nu	Nusselt number, dimensionless
p	gas pressure, Pa
p_r	gas pressure, Pa
Pr	Prandtl number, dimensionless
Q_g	heat exchanged between the particle and its external gas, J/kg/m^3
r_p	particle radius, m
R	gas constant, J/mol/K
Re_p	Reynolds number, dimensionless

R_p	polymerization rate, kg-PP/s
S_p	surface area of a particle, m^2
t	time, s
Δt	time step, s
T_g	gas temperature, K
$T_{g,i}$	inlet gas temperature, K
$T_{g,o}$	outlet gas temperature, K
T_p	particle temperature, K
$T_{p,0}$	initial particle temperature, K
u	gas velocity, m/s
u_{mf}	minimum fluidization velocity, m/s
v	particle velocity, m/s
V_g	volumetric gas flow rate, m^3/s
V_p	volume of a particle, m^3
w_c	weight of catalyst in a particle, kg
x	horizontal coordinate, m
x_n	normal overlap distance, m
x_t	tangential relative displacement, m
y	vertical coordinate, m

Greek letters

ε	voidage, dimensionless
$\varepsilon_{\text{peak}}$	peak voidage, dimensionless
η	damping coefficient, dimensionless
λ_g	thermal conductivity of gas, J/K/m/s
λ_p	thermal conductivity of particle, J/K/m/s
μ	friction coefficient, dimensionless
μ_g	gas viscosity, Pa s
ρ_g	gas density, kg/m^3
ρ_p	particle density, kg/m^3
σ	standard deviation at $t = t$, dimensionless
σ_0	standard deviation before mixing, dimensionless
σ_r	standard deviation based on the final concentration, dimensionless
ω	angular velocity, 1/s

Appendix A

For the gas phase, the following Anderson and Jackson's equations (1967) are applied:

Equation of continuity:

$$\frac{\partial \varepsilon}{\partial t} + \frac{\partial(\varepsilon u_i)}{\partial x_i} = 0 \tag{A.1}$$

Gas momentum equation:

$$\rho_g \frac{\partial(\varepsilon u_i)}{\partial t} + \rho_g \frac{\partial(\varepsilon u_i u_j)}{\partial x_j} = -\varepsilon \frac{\partial \rho_i}{\partial x_i} - f_i + \varepsilon \rho_g g \tag{A.2}$$

where ε is the local mean voidage, u_i is the local mean velocity of the gas phase, ρ_g is the gas density, t is time, p_i is the local mean gas pressure and f_i is the gas–particle interaction force.

For particle motion in a fluidized bed, the following equation is used:

Force balance:

$$m\frac{\mathrm{d}v}{\mathrm{d}t} = -mg + F_{pi} - V_p \nabla p_i + F_n + F_t \tag{A.3}$$

Rotation:

$$I\frac{\mathrm{d}\omega}{\mathrm{d}t} = |F_t| r_p \tag{A.4}$$

where m is the particle weight, g is the gravity constant, V_p is the volume of a particle, p_i is gas pressure, I is the moment of inertia, ω is the angular velocity, r_p is the particle radius, F_{pi} is the gas–particle interaction force acting on a particle and F_n and F_t are, respectively, the normal and the tangential components of the soft sphere contact interaction forces.

Due to estimation of the interaction forces of the soft sphere contact, Hook's simple linear spring and dash pot model for both normal and tangential components, assuming Coulomb's law of friction, was adopted.

For the particle–particle interaction, the force is calculated by Eqs. (A.5)–(A.8):

Normal force:

$$F_n = kx_n - \eta\frac{\mathrm{d}x_n}{\mathrm{d}t} \tag{A.5}$$

Tangential force:

$$F_t = kx_t - \eta\frac{\mathrm{d}x_t}{\mathrm{d}t} \qquad |F_t| \leqslant \mu |F_n| \tag{A.6}$$

$$F_t = \mu |F_n| \frac{x_t}{|x_t|} \qquad |F_t| > \mu |F_n| \tag{A.7}$$

$$\eta = \frac{-2\ln(e)}{\sqrt{\pi^2 + (\ln(e))^2}} \tag{A.8}$$

where η is the damping coefficient, e is the restitution coefficient, μ is the friction coefficient, x_n is the normal displacement, x_t is the tangential displacement and k is the spring constant.

For the particle–gas interaction, the force acting on a fluid cell f_i in Eq. (A.2) is calculated by Eq. (A.9) derived from Ergun's correlation for $\varepsilon < 0.8$ or for $\varepsilon \geqslant 0.8$ by Eq. (A.10) derived from Wen–Yu's correlation.

$$f_i = \left(150\frac{(1-\varepsilon)^2}{\varepsilon^2}\frac{\mu_g(u-\bar{v})}{d_p^2} + 1.75\frac{1-\varepsilon}{\varepsilon}\frac{\rho_g(u-\bar{v})|u-\bar{v}|}{d_p}\right) \qquad (\varepsilon < 0.8) \tag{A.9}$$

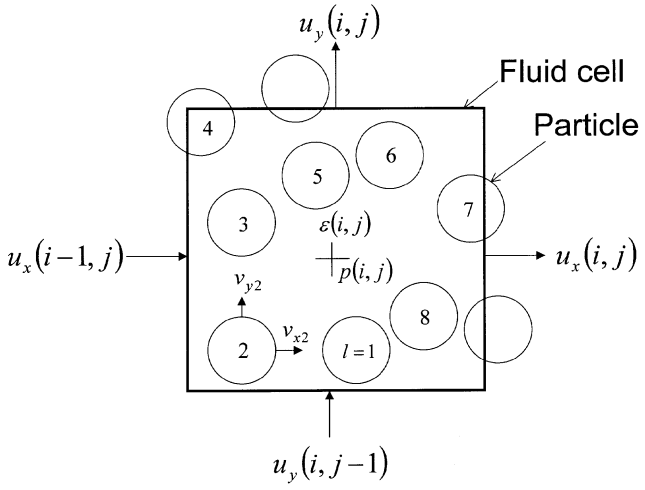

Fig. 11. Variables defined in a fluid cell.

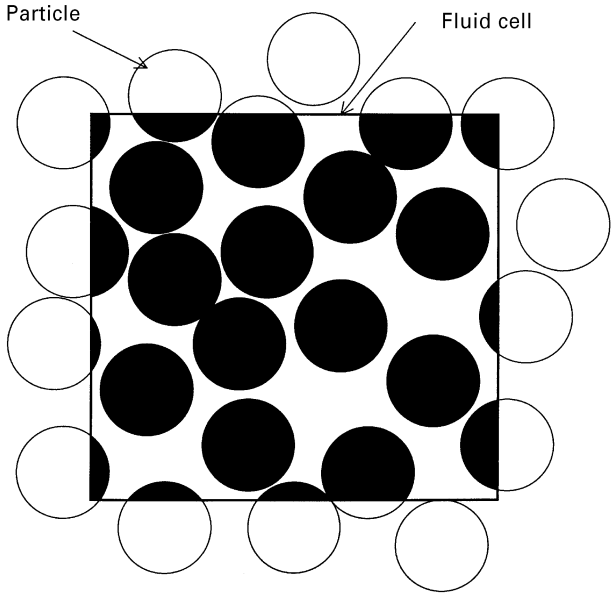

Fig. 12. Computation method for calculating the voidage (black part is the particle volume for calculating the voidage).

$$f_i = \sum_l \frac{\pi}{8} C'_{Dl}\,\rho_g \varepsilon^2 (u - v_l)|u - v_l| d_p^2 \quad (\varepsilon \geqslant 0.8) \tag{A.10}$$

$$C'_{Dl} = \varepsilon^{-4.65}\frac{24}{Re_l}(1 + 0.15\,Re_l^{0.687}) \quad (Re_l < 1000) \tag{A.11}$$

$$C'_{Dl} = \varepsilon^{-4.65} 0.44 \quad (Re_l \geqslant 1000) \tag{A.12}$$

where $Re_l = (\rho_g \varepsilon d_p|u - v_l|)/\mu_g$, μ_g is the gas viscosity, C'_D is the modified drag coefficient, $\bar{v}$ is the averaged particle velocity in a fluid cell and v_l is the velocity of an individual particle. F_{pi} in Eq. (A.3) is calculated by dividing f_i of Eq. (A.9) or Eq. (A.10) by the number of particles in the relevant cell.

Fig. 11 shows the definition of a fluid cell. Both voidage and gas pressure are defined at the center of a fluid cell, whereas the gas velocity is defined at the center of the boundary plane between cells for numerical stability (staggered grid).

In Eq. (A.9) the terms $(u - \bar{v})$ and $|u - \bar{v}|$ are calculated by the following equations:

$$(u - \bar{v})_x = 0.5(u_x(i,j) + u_x(i-1,j)) - \frac{1}{n_c}\sum_l v_{xl} \tag{A.13}$$

$$(u - \bar{v})_y = 0.5(u_y(i,j) + u_y(i,j-1)) - \frac{1}{n_c}\sum_l v_{yl} \tag{A.14}$$

$$|u - \bar{v}| = \{(u - \bar{v})_x^2 + (u - \bar{v})_y^2\}^{1/2} \tag{A.15}$$

where $(u - \bar{v})_x$ and $(u - \bar{v})_y$ are the x and y components of the relative velocities between gas and particle, respectively, n_c is the number of particles in a fluid cell v_{xl} and v_{yl} are the x and y velocity components of particle l, respectively.

To evaluate ∇p_i in Eq. (A.3) it is assumed that the pressure gradient is approximately equal to that in a stationary suspension of voidage ε. This corresponds to an assumption that the acceleration term of the gas element is negligible compared with other terms. The left-hand side of Eq. (A.2) is then nearly equal to 0 and we obtain:

$$V_p \nabla p_i = V_p\left(-\frac{f_i}{\varepsilon} + \rho_g g\right) = \frac{1-\varepsilon}{n}\left(-\frac{f_i}{\varepsilon} + \rho_g g\right) \tag{A.16}$$

where n is the number density of the particles. The same procedure was adopted by Mikami et al. (1998), although they did not discuss it clearly. Because the objective of the present work is to investigate the temperature behavior of gas-phase polymerization reactors, the development or further improvement of the DEM model is outside of our present focus.

Appendix B

The voidage was obtained by subtracting the sum of the volume of particles from the volume of a fluid cell as shown in Fig. 12. When a particle overlaps more than one neighboring cell, the volume of its part included in a particular fluid cell is taken into account to calculate the voidage of the cell.

References

Anderson, T. B., & Jackson, R. (1967). A fluid mechanical description of fluidized beds. *I & EC Fundamentals*, *6*, 527–539.

Floyd, S., Choi, K. Y., Taylor, T. W., & Ray, W. H. (1986a). Polymerization of olefins through heterogeneous catalysis. IV. Modeling of heat and mass transfer resistance in the polymer particle boundary layer. *Journal of Applied Polymer Science*, *31*, 2231–2265.

Floyd, S., Choi, K. Y., Taylor, T. W., & Ray, W. H. (1986b). Polymerization of olefins through heterogeneous catalysis. III. Polymer particle modeling with an analysis of intraparticle heat and mass transfer effects. *Journal of Applied Polymer Science*, *32*, 2935–2960.

Floyd, S., Heiskanen, Tomi, Taylor, T. W., Mann, G. E., & Ray, W. H. (1987). Polymerization of olefins through heterogeneous catalysis. VI. Effect of particle heat and mass transfer on polymerization behaviour and polymer properties. *Journal of Applied Polymer Science*, *33*, 1021–1065.

Hutchinson, R. A., & Ray, W. H. (1990). Polymerization of olefins through heterogeneous catalysis. VIII. Monomer sorption effects. *Journal of Applied Polymer Science*, *41*, 51–81.

Hutchinson, R. A., & Ray, W. H. (1991). Polymerization of olefins through heterogeneous catalysis. The effect of condensation cooling on particle ignition. *Journal of Applied Polymer Science*, *43*, 1387–1390.

Hutchinson, R. A., Chen, C. M., & Ray, W. H. (1992). Polymerization of olefins through heterogeneous catalysis. X: Modeling of particle growth and morphology. *Journal of Applied Polymer Science*, *44*, 1389–1414.

McKenna, T. F., Dupuy, J., & Spitz, R. (1995). Modeling of transfer phenomena on heterogeneous Ziegler catalysts: Differences between theory and experiment in olefin polymerization (an introduction). *Journal of Applied polymer Science*, *57*, 371–384.

McKenna, T. F., Barbotin, F., & Spitz, R. (1996). Modeling of transfer phenomena on heterogeneous Ziegler catalysts. II. Experimental investigation of intraparticle mass transfer resistance during the polymerization of ethylene in slurry. *Journal of Applied Polymer Science*, *62*, 1835–1841.

McKenna, T. F., Dupuy, J., & Spitz, R. (1997). Modeling of transfer Phenomena on heterogeneous Ziegler catalysts. III. Modeling of intraparticle mass transfer resistance. *Journal of Applied Polymer Science*, *63*, 315–322.

Mikami, T., Kamiya, H., & Horio, M. (1998). Numerical simulation of cohesive powder behavior in a fluidized bed. *Chemical Engineering Science*, *53*, 1927–1940.

Montedison (1985). *US patent* 4518750.

Muguruma, Y., Tanaka, T., Kawatake, S., & Tsuji, Y. (1996). Discrete particle simulation of rotary vessel mixer with baffles. *Journal of Mechanical Society of Japan*, *62-601(B)*, 3335–3340.

Ranz, W. E. (1952). Friction and transfer coefficients for single particles and packed beds. *Chemical Engineering Progress*, *48*, 247–253.

Raufast, C.R. (1984). Process details of BP Chimie's LLDPE. *Hydrocarbon Processing*, May 105–108.

Satoh, M., Deguchi, Y., Komura, S., & Miyanami, K. (1985). The development of a continuous measuring system for the degree of mixing of powders by an optical method. *Journal of the Society of Powder Technology Japan*, *22*, 79–84.

Showadenko (1991). *Japan patent Kokai* 153703.

Sumitomo (1997). *Japan patent* 2722969.

Tsuji, Y., Kawaguchi, T., & Tanaka, T. (1993). Discrete particle simulation of two-dimensional fluidized bed. *Powder Technology*, *77*, 79–87.